LAWRENCE
LIVERMORE
NATIONAL
LABORATORY

UCRL-JRNL-226939

Simulations of X-ray Emission from Omega Fill Tube Experiments

S. Langer, N. Izumi, T. Dittrich, S. Haan

December 20, 2006

High Energy Density Physics

Disclaimer

This document was prepared as an account of work sponsored by an agency of the United States Government. Neither the United States Government nor the University of California nor any of their employees, makes any warranty, express or implied, or assumes any legal liability or responsibility for the accuracy, completeness, or usefulness of any information, apparatus, product, or process disclosed, or represents that its use would not infringe privately owned rights. Reference herein to any specific commercial product, process, or service by trade name, trademark, manufacturer, or otherwise, does not necessarily constitute or imply its endorsement, recommendation, or favoring by the United States Government or the University of California. The views and opinions of authors expressed herein do not necessarily state or reflect those of the United States Government or the University of California, and shall not be used for advertising or product endorsement purposes.

LAWRENCE
LIVERMORE
NATIONAL
LABORATORY

UCRL-JRNL-226939

Simulations of X-ray Emission from Omega Fill Tube Experiments

S. Langer, N. Izumi, T. Dittrich, S. Haan

December 20, 2006

High Energy Density Physics

Disclaimer

This document was prepared as an account of work sponsored by an agency of the United States Government. Neither the United States Government nor the University of California nor any of their employees, makes any warranty, express or implied, or assumes any legal liability or responsibility for the accuracy, completeness, or usefulness of any information, apparatus, product, or process disclosed, or represents that its use would not infringe privately owned rights. Reference herein to any specific commercial product, process, or service by trade name, trademark, manufacturer, or otherwise, does not necessarily constitute or imply its endorsement, recommendation, or favoring by the United States Government or the University of California. The views and opinions of authors expressed herein do not necessarily state or reflect those of the United States Government or the University of California, and shall not be used for advertising or product endorsement purposes.

This work was performed under the auspices of the U. S. Department of Energy by University of California, Lawrence Livermore National Laboratory under Contract W-7409-Eng-48.

Simulations of X-ray Emission from Omega Fill Tube Experiments

Steven H. Langer[a,*], Nobuhiko Izumi[a], Thomas R. Dittrich[a], and Steven W. Haan[a]

[a]Lawrence Livermore National Laboratory, Livermore, CA 94550

Abstract

The capsules used in ignition experiments on the National Ignition Facility (NIF) laser will have a layer of frozen DT inside a low-Z shell. Liquid DT will be injected through a narrow fill tube that penetrates the shell and frozen in place. The fill tube is a perturbation on the surface of the capsule and hydrodynamic instabilities will cause this perturbation to grow during an implosion. Experiments to investigate the growth of perturbations due to fill tubes have been carried out on the Omega laser. The goal of these experiments was to validate simulations at Omega energy scales and thus increase confidence in the use of simulations in planning for NIF experiments. Simulations show that the fill tube leads to a jet of shell material that penerates into the DT fuel. Simulations will be used to pick experimental conditions in which the jet is small enough that it does not significantly reduce the yield of a NIF implosion. This paper compares experiments in which bumps and stalks were used as fill tube surrogates to 2D simulations of x-ray emission from Omega capsule implosions. Experiments and simulations are in reasonable agreement on the size of a bump or stalk required to produce a jet that is visible above the emission from a (nominally) smooth capsule.

Keywords: Radiative Transfer; Inertial Confinement Fusion

* Corresponding Author. *E-mail address*: langer1@llnl.gov

1. INTRODUCTION

Inertial confinement fusion (ICF) implosions are designed to be spherical to maximize the compression and heating of the fuel (D_2) in the experiments

discussed here). Capsules always have surface imperfections and the drive is never perfectly symmetric. These departures from spherical symmetry are amplified by hydrodynamic instabilities and can lead to decreased thermonuclear yield. The situation is further complicated by the need to fill the interior of the capsule with cryogenic fuel in National Ignition Facility (NIF) experiments. The first ignition experiments planned at the NIF will inject liquid DT via a fill tube that pierces the capsule shell and then carefully freeze the DT to produce a smooth layer on the inside of the shell.

Experiments performed in 2004-6 using the Omega laser at the University of Rochester used bumps or stalks placed on the capsule surface rather than fill tubes. Future experiments at Omega will use tubes that penetrate the shell. Simulations show that bumps, stalks, and fill tubes of equal mass have similar effects so these experiments are helpful in validating our modeling capabilities. The techniques developed to model the Omega experiments will be used to plan future experiments on the NIF laser.

An experimental signature of the effects of a bump or stalk is required for these experiments to be successful. The approach used in the Omega experiments is to measure x-ray emission from the innermost layer of the ICF capsule. A small amount of titanium, 1.6% by number, was placed in the inner layer of the plastic shell to enhance emission. Titanium emission is weak if the jet is small (all the plastic remains cool). If the jet extends in a significant fraction of the distance between the shell and the center of the fuel, the material in the jet becomes hotter and is brighter in x-ray images.

Asymmetries in the x-ray drive or imperfections on the capsule surface may also cause shell material to push a significant fraction of the capsule radius into the fuel. This material will be hotter and emit more x-rays than in the spherical case. Emission due to the fill tube should consist of a narrow jet aligned with the known

initial location of the fill tube. Emission due to other perturbations should be spread around the capsule surface. The differences in spatial distribution of the different sources of emission mean that x-ray images are a better diagnostic than x-ray spectra. The bump or stalk must be large enough that the emission from the resulting jet is bright enough to be seen above the emission resulting from surface roughness.

Earlier papers [1,2,3,4,5] have discussed the development of simulation tools that can accurately model atomic line emission from ICF capsules. In this paper we use the same simulation tools to model both line and continuum x-ray emission. The detector must collect both line and continuum emission to obtain an adequate signal-to-noise ratio in images with shutter times of roughly 60 ps.

2. THE MODELING PROCEDURE

The experiments simulated in this paper are all indirect drive ICF implosions carried out on the Omega laser at the University of Rochester. In these experiments, laser light was converted to x-rays by heating a gold hohlraum. Some of the x-rays fall on the capsule and ablate shell material. The simulations presented in this paper do not model the hohlraum – they use an x-ray source derived from a separate hohlraum simulation.

The various layers in the capsule are shown in Fig. (1). Titanium (1.6% by number) was placed in the innermost part of the plastic shell. The titanium concentration was low enough that it did not change the implosion hydrodynamics. There was no argon in the central gas, in contrast to the experiments discussed in [1-5]. The capsules did not have germanium as a pre-heat shield and had relatively high fill pressures (50 atm) so the convergence of the shell was not as high as in the experiments discussed in our earlier papers [1-5].

Fig. (2) shows the capsule inside the hohlraum and the diagnostic holes in the walls of the hohlraum. The pinholes for the framing camera are mounted on the hohlraum to obtain high (90X) magnification. The bump or stalk is on the limb of the capsule when viewed by the framing camera (XRFC3). The image plate diagnostic (IPD) and streaked crystal spectrometer (SSCA) were fielded during these experiments, but their data has not been analyzed.

The bumps and stalks deliberately placed on the surface and surface imperfections both grow on the outer surface due to the Rayleigh-Taylor instability [6] [7] during the inward acceleration of the capsule and feed through to perturb the inner surface. Perturbations at the inner surface grow due to the Rayleigh-Taylor instability when the shell decelerates near the time of peak compression. Richtmeyer-Meshkov instabilities [8] [9] occur as shocks pass through the capsule and serve as a seed for Rayleigh-Taylor instabilities.

Deleted: 7

Deleted: 8

Deleted: 9

Deleted: 10

The hohlraum is driven by a 2.3 ns laser pulse with 13 kJ of 0.35 μm light. There is an intensity contrast of 5 between the low intensity foot of the pulse and the main drive x-rays. These simulations do not include the effects of drive asymmetry.

The Lasnex radiation-hydrodynamics code [10] was used to simulate the implosion. Lasnex is a 2D code, so the bump was placed as one pole of the capsule. Random surface perturbations with a root-mean-square (RMS) amplitude of 0.025 μm and a spectrum based on capsule measurements were applied. This roughness is similar to that measured for capsules used in the experiments. Photographs of capsules sometimes show isolated bumps in addition to the overall surface roughness. These simulations do not include the effects of isolated bumps.

The Lasnex grid covered a full sphere and had roughly 250 azimuthal points and 200 radial points. The Lasnex models used 57 frequencies. Lasnex uses a Lagrangean hydrodynamics package, but the simulations were rezoned whenever grid distortions became large.

The XSN average atom model [11] in Lasnex was used to generate time-dependent opacities and emissivities. X-ray emission is modeled by first running the Lasnex radiation-hydrodynamics code to compute opacities and emissivities. The radiation transport equation was then solved on a grid of rays through this opacity and emissivity to generate simulated x-ray images. Most of the x-rays passing through the filter of the framing camera are continuum radiation so there is no need for detailed opacities such as the Ration opacities used in [1-5].

Deleted: 12

3. RESULTS

The titanium emission comes from a very thin layer of material on the inside of the shell where the plastic is warm enough for titanium lines and continuum to be emitted. Distortions in the fuel-shell interface will bring some of the titanium closer to the hot fuel at the center and increase the rate at which heat is conducted from the fuel into the shell. This additional heat raises the temperature and increases titanium emission.

Earlier studies of the growth rates of single perturbation modes have shown that the modes $l \bullet 40$ are responsible for most of the amplitude of the distortions in the interface [12]. The surface roughness and the bump on the capsule both are made up from many l-modes. We have directly simulated the non-linear, coupled growth of these modes. Higher l-modes have a product of initial amplitude and linear growth factor that is smaller than for the l-modes that were simulated. Saturation effects will further reduce the contribution of high-l modes to the interface distortion. We believe that the current simulations include all the l-

modes that will have a significant effect on the fusion yield and the x-ray emission from these implosions.

Deleted: ¶
---------- figs. 4 and 5 should be semi-log¶

The yield drops when cold material pushes into the hot spot because heat is conducted out of the fuel. The perturbations in these experiments are small enough that their effect on yield cannot be distinguished from normal shot-to-shot variations.

The principal diagnostic for these experiments is an x-ray framing camera. The camera had 90x magnification and a spatial resolution of 7 um (the size of the pinholes). The images from roughly 8 pinholes fall on each of the 4 striplines in the framing camera. The shutter time of an individual image is approximately 60 ps and the striplines overlap slightly in time. The detector had a filter consisting of 31 mil of Be. The capsule was viewed through a patch on the hohlraum wall consisting of 25 μm of beryllium with an overcoat of 0.2 μm tantalum. A Lasnex simulation of the hohlraum was used to obtain the attenuation through this patch at the time the capsule images were recorded. The unattenuated spectrum from the capsule is shown by the thick solid line in Fig. (3). The thin solid line shows the energy dependence of the spectrum after attenuation by the patch on the hohlraum wall and the filter on the detector. The quantum efficiency of the detector is not included, but it is relatively flat between 2 and 8 keV. Most of the transmitted x-rays are between 2 and 4 keV. The first experiments in this series used a filter that included some titanium (dashed line in fig. 3) and it allowed far less signal through than our current filter. Simulations show that the continuum above 2 keV comes from the titanium doped layer so “opening up” the filter does not compromise our ability to measure the location of the interface between the shell and the D_2 gas.

Simulated x-ray images are obtained from ray traces through the opacities calculated by Lasnex and include the filter attenuation shown in Fig. (3) and the

quantum efficiency of the detector. The absolute normalization of the detector is uncertain by roughly a factor of two (the quantum efficiency is calculated, not measured), but the energy dependence is known fairly accurately. The images are blurred to account for the size of the pinhole and fluctuations due to Poisson counting statistics are added. Including the counting statistics when simulating images was helpful in determining which filter to use.

The simulations were run in two dimensions (RZ), but the x-ray images are generated in three dimensions by assuming azimuthal symmetry. A bump on the surface of a 2D capsule becomes a circular ridge in 3D and appears as a "bar" in the side-on view used for the simulated x-ray images. The exception is the deliberately imposed bump or stalk at the pole of the capsule – it is also a bump in 3D. If the implosion were simulated with a 3D code, the surface roughness would produce bright spots instead of bars of emission. The total emission in the 2D bars and the 3D spots are similar for capsules with the same surface roughness.

Fig. (4a) shows experimental images at 5 times for a capsule with a 51 μm wide by 4.5 μm high bump. Fig. (4b) shows experimental images at 5 times for a capsule with a 29 μm diameter stalk. The images are normalized so that the brightest pixel in each group of 5 images is at the top of the grayscale. The bump and stalk are initially at the bottom of the capsule. The jet moves upward from frame to frame and is in the expected vertical direction. The x-rays are bright for roughly 100 ps.

Deleted: 8

Fig. (5a) shows simulated images at 5 times for a capsule with a 55x3 μm bump. Fig. (5b) shows simulated images at 5 times for a capsule with a 29 μm stalk. The jet motion is similar to that seen in the experimental images in fig. (4a) and (4b). In these figures, each image is normalized to extend to the top of the color bar. The x-rays are bright for roughly 100 ps (as in the experiment), but this is not visually apparent due to the choice of normalization.

Fig. (6a) shows time-integrated images for 4 capsules with bumps. Each image is normalized so that its brightest pixel is at the top of the color bar (the peak brightness is greater for larger bumps). The capsule with no deliberately imposed perturbation and the capsule with the deliberate 54x1.6 μm bump do not show obvious jets. An examination of the time dependence for these two capsules shows that the bright spots do not move significantly during the experiment. The images for the capsules with the two larger bumps show obvious jets in the expected vertical direction. Fig. (6b) shows time-integrated images for 4 capsules with stalks. The capsules with small stalks have bright spots but do not have an observable jet. The larger stalks produce jets very similar to those from the larger bumps in fig. (6a).

The nearly stationary bright spots seen in images of the capsules with small deliberately imposed perturbations appear to correlate with the positions of unintentional imperfections on the capsule surface.

Fig. (7) shows time-integrated simulated images for the 4 different stalk sizes shown in fig. (6b). Fig. (8) has line-outs along the jets in the images shown in fig. (7). The extent of the jet is larger for the two capsules with large stalks. The length of a jet in a time-integrated image might be useful in making quantitative comparisons between experiment and simulation.

No jet was visible in the experimental images for the smaller bump and the two smallest stalks in fig. (4). This does not mean the perturbation failed to cause a jet – the jet probably wasn't as bright as the emission due to unintentional bumps on the capsule surface. Fig. (9) shows simulated images for two capsules with 55x3 and 55x1.5 μm bumps. In a 3D simulation the bands of emission would break up into individual bright spots with an average brightness similar to the average brightness in the 2D simulation. The net result is that it would be difficult to see

the jet in a simulated image of a capsule with a 55x1.5 μm bump. The size of a bump that produces a jet visible above the background due to surface roughness is similar in experiment and simulation.

Streaked spectra were recorded during these experiments. The spectral dispersion was obtained using a PET crystal. The emission was fairly weak and has not yet been analyzed in detail.

4. CONCLUSIONS

Jets due to both bumps and stalks serving as surrogates for a fill tube have been seen in experiments on the Omega laser. The appearance of the jet is similar to that predicted by simulations. Experiment and simulation are in reasonable agreement on the size of a bump that is required to create a jet that is visible above the background emission from the plastic shell. In future experiments we hope to obtain high quality time-integrated images using image plates. The length of the jets could be measured for a variety of stalk sizes. These results could be compared to the lengths predicted by simulations to provide a quantitative comparison between experiment and simulation.

Acknowledgements

This work was performed under the auspices of the U.S. Department of Energy by the University of California Lawrence Livermore National Laboratory under contract No. W-7405-Eng-48.

REFERENCES

1. Keane, CJ, Pollak, GW, Cook, RC, Dittrich, TR, Hammel, BA, Landen, OL, Langer SH, Levedahl, WK, Munro, DH, Scott HA, and Zimmerman, GB. X-ray spectroscopic diagnostics of mix in high growth factor spherical implosions. J Quant Spectrosc Radiat Transfer 1995; 54:207-220.

Formatted: Bullets and Numbering

2. Langer SH, Scott HA, Keane, CJ, Landen, OL, and Marinak MM. Yield and emission line ratios from ICF target implosions with multi-mode Rayleigh-Taylor perturbations. J Quant Spectrosc Radiat Transfer 1997; 58:709-720.

3. Langer SH, Scott HA, Marinak MM, and Landen OL. Towards a complete model of 3D line emission from ICF capsules: results from the first 3D simulations. J Quant Spectrosc Radiat Transfer 2000; 65:353-366.

4. Langer SH, Scott HA, Marinak MM, and Landen OL. Modeling titanium line emission from ICF capsules in three dimensions. J Quant Spectrosc Radiat Transfer 2001; 71:479-492.

5. Langer SH, Scott HA, Marinak MM, and Landen OL. Comparisons of line emission from 2- and 3-dimensional simulations of ICF capsules to experiments. J Quant Spectrosc Radiat Transfer 2003; 81:275-286.

6. Lord Rayleigh. Scientific Papers, Vol. II, p. 200. Cambridge University Press, 1990.

7. Taylor GI. Proceedings of the Royal Society of London Ser. A 1950; 201:192.

8. Richtmyer RD. Communications on Pure and Applied Mathematics 1960; 13:297.

9. Meshkov EE. Izv. Akad. Nauk. SSSR. Mekh. Zhidk. Gaz 1969; 5:151 (NASA TTF-13-074, 1970).

10. Zimmerman GB, and Kruer WL. Communications on Plasma Physics and Controlled Thermonuclear Fusion 1975; 2:51.

11. Lokke WA, and Grassberger WH, Lawrence Livermore National laboratory Report No. UCRL-52276, 1977 (unpublished).

12. Marinak MM, Tipton RE, Landen OL, Murphy TJ, Amendt P, Haan SW, Hatchett SP, Keane CJ, McEachern R, and Wallace R. Physics of Plasmas 1996; 3:2070.

Formatted: Bullets and Numbering

Figure Captions

Fig. (1). The capsule consists of a plastic shell filled with D_2 gas. The inner layer of the shell has a small amount of titanium to serve as a spectroscopic tracer.

Fig. (2). The capsule is mounted inside a hohlraum. The capsule is viewed through a beryllium patch on the side of the hohlraum. The pinholes are mounted on a stalk attached to the hohlraum so that high magnification (90X) can be obtained.

Fig. (3). The thick solid curve shows the (spatially integrated) spectrum from the capsule near the time of peak compression. The signal is attenuated when passing through the patch on the hohlraum and the filter on the front of the detector. The thin solid curve shows the signal after passing through the 30 mil beryllium filter. Most of the signal is due to photons between 2 and 4 keV. The titanium line at 4.75 keV and the titanium free-bound continuum above 6 keV are also visible. Almost all emission above 2 keV comes from the thin, titanium-containing layer on the inside of the shell.

Fig. (4a). The images show the jet resulting from a 52x4.5 µm bump at 5 times. The jet moves steadily upward and reaches the far side of the capsule around 3 ns. The bump is originally at the bottom of the capsule.

Fig. (4b). The images show the jet resulting from a 29 µm diameter stalk at 5 times. The jet moves steadily upward. The stalk is originally at the bottom of the capsule.

Fig. (5a). Simulated images of the jet resulting from a 55x3 µm bump are shown at 5 times. All images are normalized to use the full extent of the color bar. The x-rays are only bright for roughly 100 ps as in the experiment. Each image is 80 µm across. The emission due to surface roughness becomes relatively brighter late in time.

Fig. (5b). Simulated images of the jet resulting from a 14 µm stalk are shown at 5 times. The images are similar to those in fig. (5a) except that surface roughness was not included in this simulation.

Fig. (6a). Time-integrated images of a smooth capsule and capsules with 54x1.6 µm, 51x4.5 µm, and 46x7.6 µm bumps are shown. The jet is clearly visible for the two capsules with large bumps. The bright spots in the two other images are probably due to surface roughness and obscure the emission from the relatively small jet due to the deliberate bump.

Fig. (6b). Time-integrated images of capsules with 9 µm, 14 µm, 29 µm, and 37 µm diameter stalks are shown. The jet is clearly visible for the two capsules with large stalks. The bright spots in the two other images are probably due to surface

roughness and obscure the emission from the relatively small jet due to the deliberate bump.

Fig. (7). Time-integrated simulated images of capsules with 9 µm, 14 µm, 29 µm, and 37 µm diameter stalks are shown. The jet is clearly visible in all four cases. There is no emission due to surface roughness to obscure the jets in these simulations.

Fig. (8). This figure shows line-outs through the time-integrated, simulated images in fig (7). The length of the jet is clearly larger for the 29 and 37 µm diameter stalks.

Fig. (9) shows time-integrated, simulated images for capsules with 55x3 µm and 55x1.5 µm bumps. The “background” emission is actually the same in both simulations, but appears different because each image has been normalized to use the full grayscale. The jet is visible in both images. If 3D simulations had been run, the emission in the horizontal bands would break up into a number of bright spots and make it difficult to see the jet.

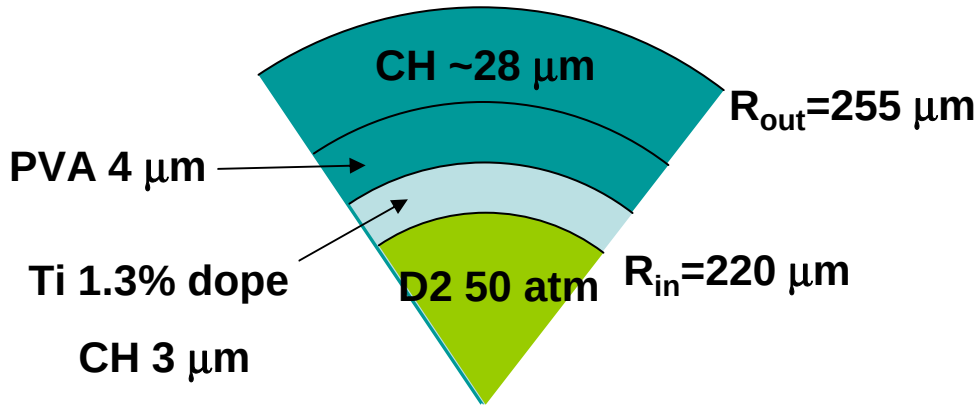

Figure 1

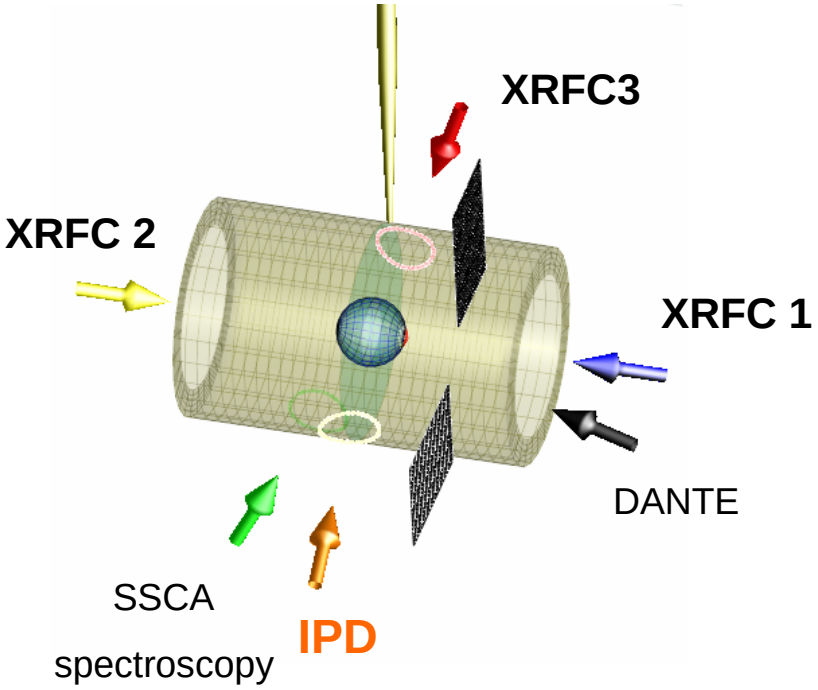

Figure 2

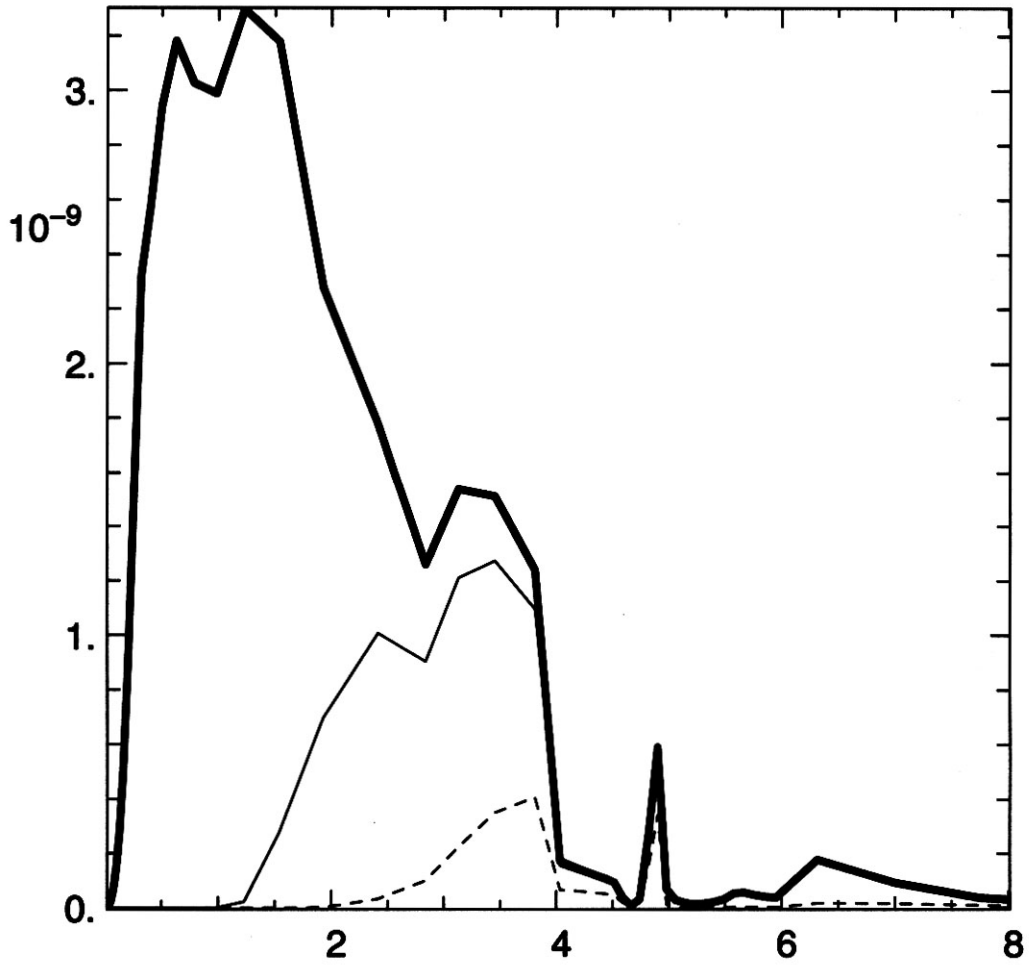

Figure 3

51x4.5 um
bump

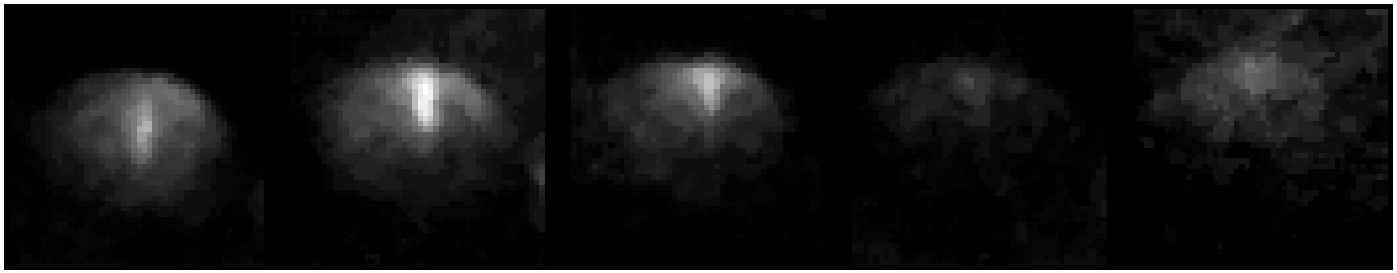

2.89 ns 2.91 ns 2.96 ns 3 ns 3.07 ns

Figure 4a

29 um
stalk

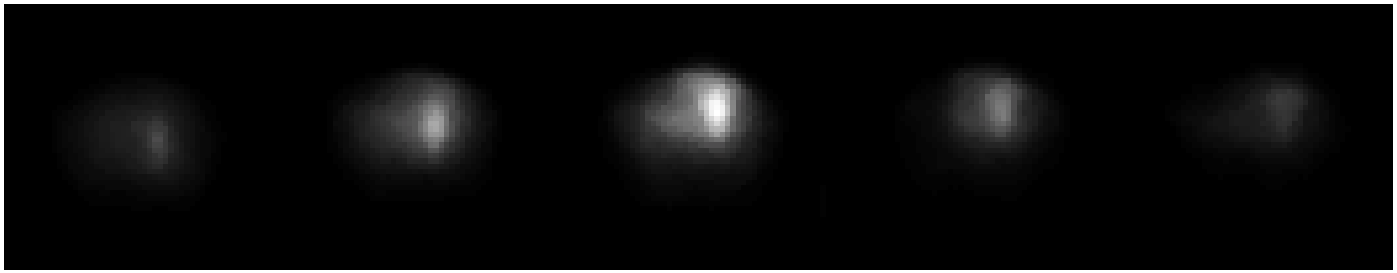

2.71 ns 2.74 ns 2.81 ns 2.84 ns 2.91 ns

Figure 4b

55x3 μm bump, ~7.5x10^{-9} cm^3

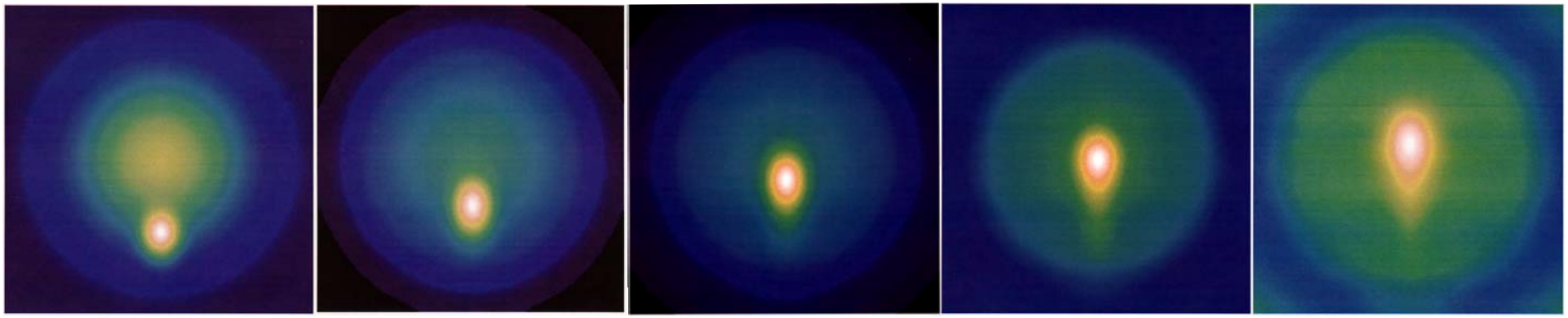

-120 -60 0 60 120

Figure 5a

Time (ps) relative to
peak x-ray emission

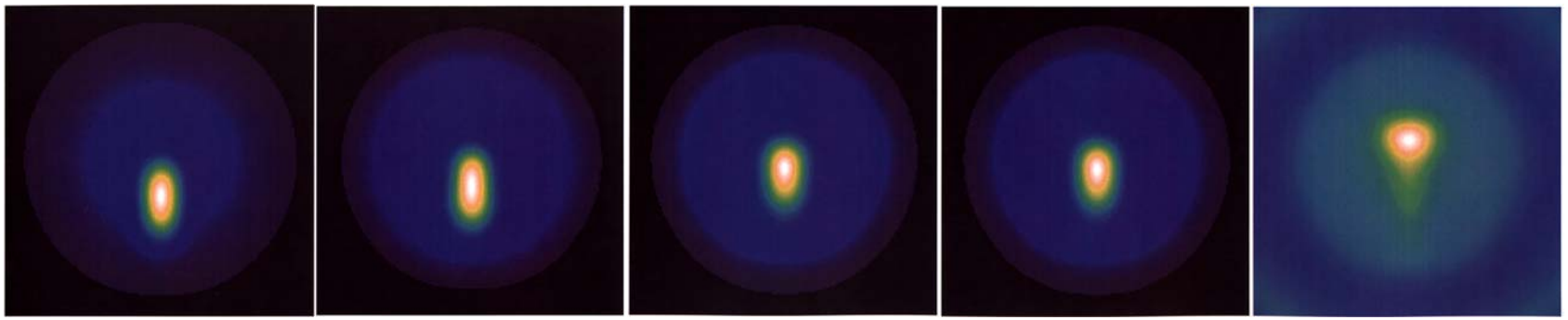

-120 ps -60 ps 0 ps 60 ps 120 ps

Figure 5b

14 μm stalk

bumps

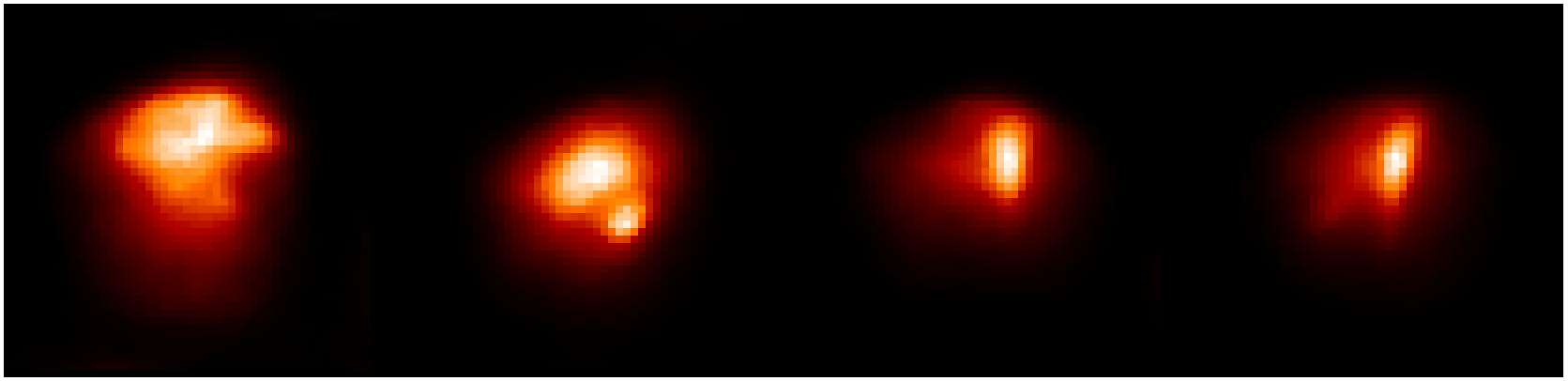

smooth 54x1.6 um 51x4.5 um 46x7.6 um

Figure 6a

stalks

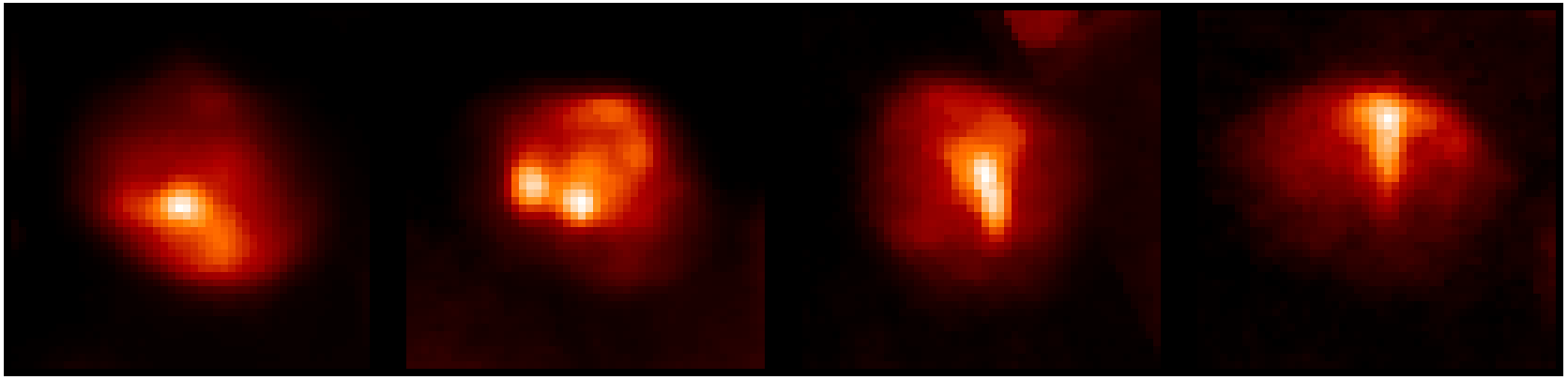

9 um 14 um 29 um 37 um

Figure 6b

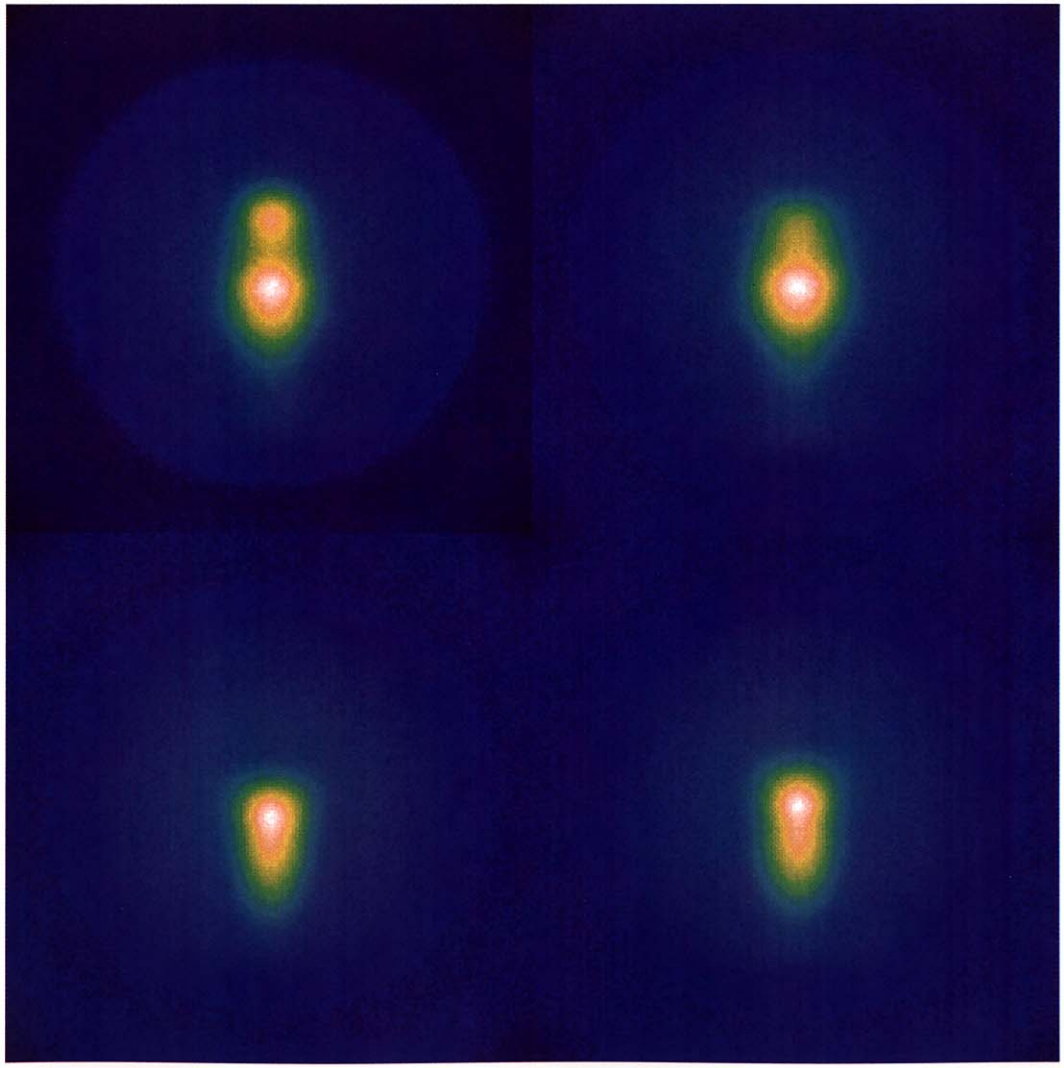

Figure 7

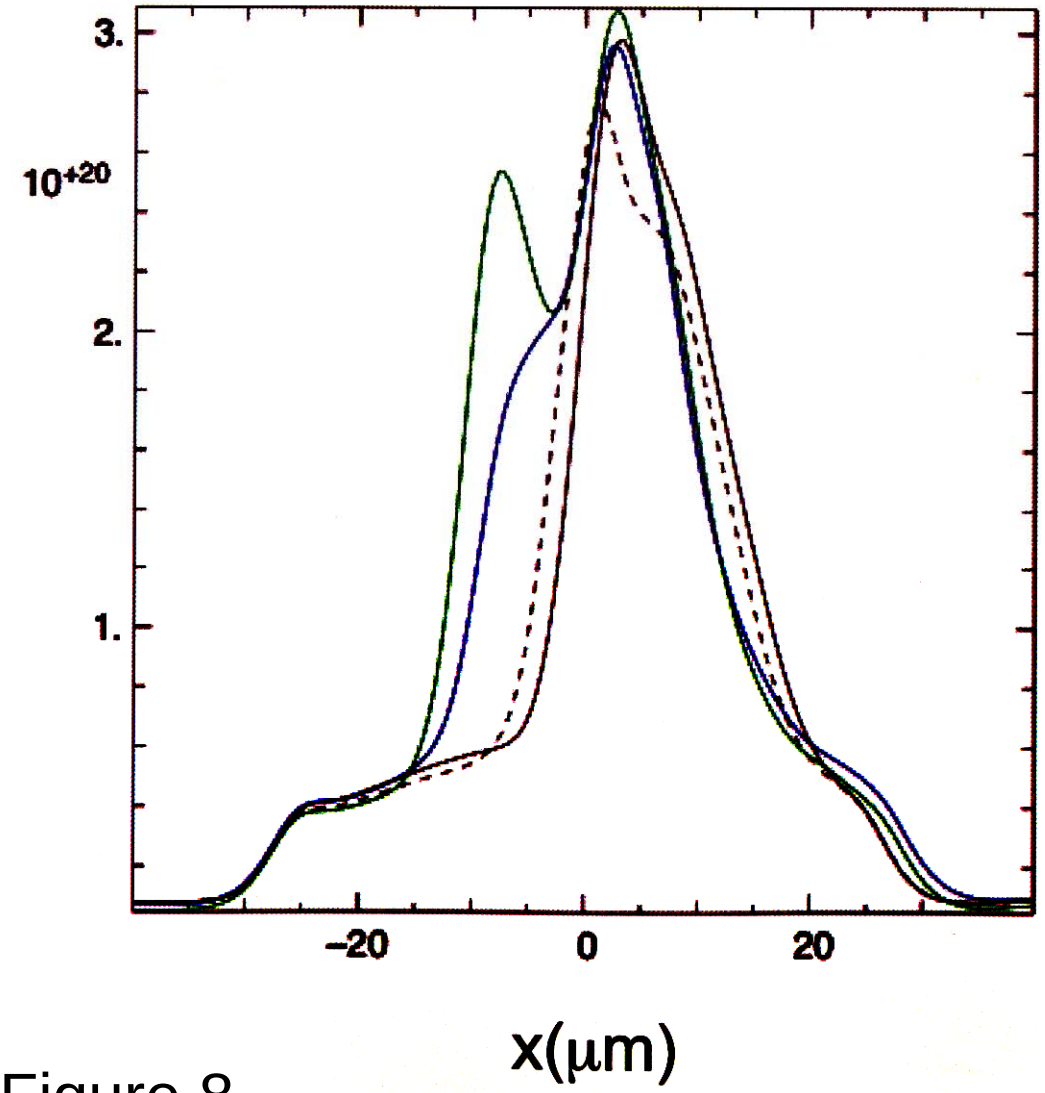

No blur
No noise

black - 9 μm
dashed - 14 μm
green - 29 μm
blue - 37 μm

Figure 8

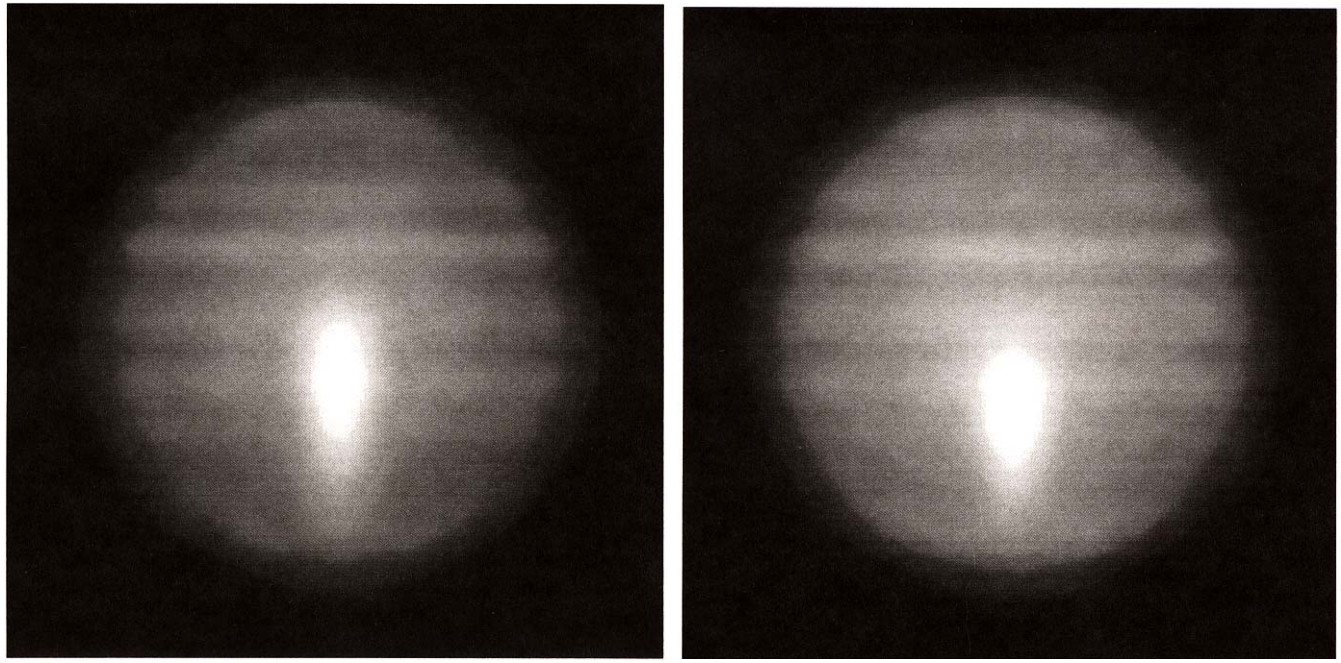

3x55 μm
(omt210)

1.5x55 μm
(omt211)

Figure 4a